Theory of Polarization-Dependent Amplification in a Slab Waveguide with Anisotropic Gain and Losses

T. D. Visser, H. Blok, and D. Lenstra

***Abstract*— We analyze the waveguiding properties of a semiconductor slab waveguide amplifier in which the gain (i.e., the permittivity) in the quantum well (QW) is taken to be anisotropic. Losses may be present simultaneously in the cladding layers. Using scattering theory, a rigorous integral equation is derived. Our model incorporates the two main causes of polarization sensitivity of the amplification, viz., 1) waveguiding and 2) the anisotropic light–matter interaction in the QW. It is determined how much anisotropy is needed in the QW to get a polarization-insensitive amplification. Also, reflection coefficients and TE/TM mixing are studied. A comparison between the exact results and the Born approximation is made. A Green's tensor for a layered structure with losses is derived.**

***Index Terms*— Optical amplifiers, polarization, propagation, scattering, semiconductor lasers, waveguide theory.**

I. Introduction

A LIGHT signal that travels along an optical fiber will continuously change its state of polarization. Therefore, it is important that the amplification of weakened signals in long-haul networks is polarization-independent. The same is true for preamplifiers that are used to enhance the sensitivity of detectors. It is important to note that even in fiber amplifiers polarization effects play an important role. The reason is that both the incoming signal and the pump beam can cause polarization hole burning [1], [2].

Semiconductor optical amplifiers are an attractive alternative for fiber amplifiers because of their small size, low cost, and easy integration with other components. However, the amplification in these devices is not inherently polarization-independent. For example, we found in a previous paper [3] that, for realistic isotropic dielectric slab structures (i.e., with an active layer of $\sim$150-μm thickness and a *scalar* permittivity), the gain in decibels per length unit for TE modes can be almost twice as large as that for TM modes. It should be realized that this can happen even when the power confinement or filling factors are comparable for the two polarization states. This is explained by the fact that the often used approximation for the modal gain $g_{\mathrm{mod}} = \Gamma g_{\mathrm{bulk}}$, where Γ is the power confinement factor and g_{bulk} the bulk gain of the active layer, is highly inaccurate for TM modes under typical circumstances. This follows from the fact that the TE and the TM solutions satisfy different wave equations. For a derivation of the exact relation between confinement factors and gain, we refer to [4] and [5].

So, in order to obtain the desired polarization-insensitivity, one must use either a nonplanar device, e.g., a channel or ridge waveguide [6] or a slab waveguide with an anisotropic active layer. In this paper, we concentrate on the latter. This is inspired by the report of a high-gain polarization-insensitive semiconductor amplifier that is now available [7], [8]. This device uses several quantum wells (QW's) (of both the tensile strain and the compressive strain type) to obtain an amplification that is equal for TE and TM signals. It operates in a wavelength window around 1310 nm that is favorable for optical fiber communication.

In this paper, we model the polarization sensitivity of a semiconductor slab laser amplifier (SLA) within the linear regime. The gain in the active region is supposed to be anisotropic, i.e., the permittivity there is represented by a tensor rather than a scalar. The anisotropy of the permittivity arises through the presence of (strained) QW's. In other layers, isotropic losses may be present. We use the so-called domain integral equation method (DIEM), which has been used previously to derive guided modes of channel and ridge waveguides [9]–[12]. In this study, it is used to describe the scattering of an incident field by an anisotropic active region of a finite length: the QW. The DIEM is a rigorous approach which, unlike many approximate methods, does not suffer from drawbacks such as a finite-sized computation window, or instabilities near cut-off [13]. It is essentially a Green's function method, for which the Green's tensor for a layered structure with losses is derived. Our model allows us to investigate TE/TM mixing and obtain reflection and transmission coefficients. Also, for a certain configuration, we determine the amount of anisotropy in the active region that precisely compensates the effect of waveguiding, giving a polarization-independent amplification.

We also compare our exact results with those obtained by the Born approximation.

Manuscript received June 2, 1998; revised October 8, 1998. The work of T. D. Visser was supported by the Dutch Technology Foundation (STW). The work of H. Blok was supported by the Stichting Fund for Science, Technology, and Research (a companion organization to the Schlumberger Foundation in the U.S.).

T. D. Visser and D. Lenstra are with the Department of Physics and Astronomy, Free University, 1081 HV Amsterdam, The Netherlands.

H. Blok is with the Laboratory of Electromagnetic Research, Department of Electrical Engineering, Delft University of Technology, 2600 GA Delft, The Netherlands.

Publisher Item Identifier S 0018-9197(99)00855-6.

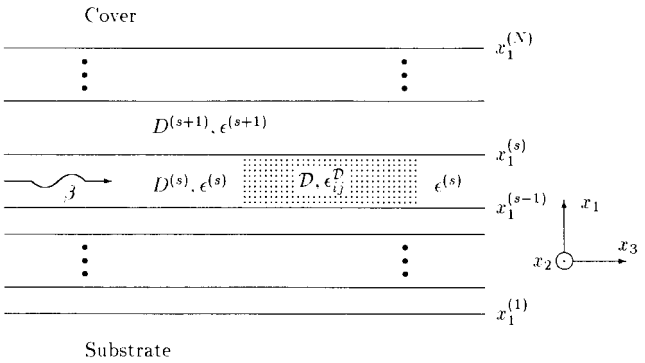

Fig. 1. Geometry of a semiconductor SLA. The domain $\mathcal{D}$ (the shaded region) indicates the active region (QW). It is completely contained within the "background layer" $D^{(s)}$. The gain in $\mathcal{D}$ is anisotropic, i.e., $\epsilon^{\mathcal{D}}$ is a tensor. The incident guided mode propagates in the positive x_3 direction with effective index β.

II. Configuration and Basic Equations

We study a configuration that is stratified in the vertical or x_1 direction (see Fig. 1). It is made up of a "background" of homogeneous and isotropic layers of dielectric material which extend from minus to plus infinity in the x_2 and x_3 directions. In layer $D^{(s)}$, however, there is a volume—finite in the x_1 and x_3 directions, infinite in the direction of x_2—of active material in which the incident wave gets amplified. This volume, which represents the QW, is called the "domain $\mathcal{D}$." The electric properties of $\mathcal{D}$ are anisotropic, i.e., the permittivity $\epsilon^{\mathcal{D}}$ is a tensor. The lowest layer of the background, the substrate, and its top layer, the cover or superstrate, are both semi-infinite in the x_1 direction. An incident field, traveling in the positive x_3 direction, is amplified in the active domain $\mathcal{D}$.

Often, so-called windows are used in which the active layer is embedded in semiconductor material in order to reduce reflectivity (similar to how the active layer $\mathcal{D}$ is embedded in $\mathcal{D}^{(s)}$ in Fig. 1). Tilted active waveguides are used for the same purpose [14].

Both the electric field $\hat{\mathbf{E}}$ and the magnetic field $\hat{\mathbf{H}}$ are written as the sum of the incident field and a scattered field

$$\{\hat{\mathbf{E}}, \hat{\mathbf{H}}\} = \{\hat{\mathbf{E}}^{\text{inc}}, \hat{\mathbf{H}}^{\text{inc}}\} + \{\hat{\mathbf{E}}^{\text{sca}}, \hat{\mathbf{H}}^{\text{sca}}\}. \tag{1}$$

The incident field satisfies the steady-state Maxwell equations for a source-free region

$$-\nabla \times \hat{\mathbf{H}}^{\text{inc}} + j\omega\epsilon^B \hat{\mathbf{E}}^{\text{inc}} = 0, \tag{2}$$

$$\nabla \times \hat{\mathbf{E}}^{\text{inc}} + j\omega\mu_0 \hat{\mathbf{H}}^{\text{inc}} = 0. \tag{3}$$

Here $\epsilon^B(x_1)$ denotes the scalar permittivity of the background configuration *without* the domain $\mathcal{D}$, i.e., with $\epsilon_{ij}^{\mathcal{D}}$ replaced by $\epsilon^{(s)}$. Just like the configuration, the field is assumed to be independent from x_2, i.e.,

$$\{\hat{\mathbf{H}}, \hat{\mathbf{E}}\} = \{\hat{\mathbf{H}}, \hat{\mathbf{E}}\}(x_1, x_3, j\omega) \tag{4}$$

hence $\partial_2 \equiv 0$. The background media are assumed to be homogeneous, isotropic, nonmagnetic, nonconducting, and linear.

The incident field is assumed to consist of TE or TM guided modes of the background configuration. That is, it is of the form

$$\{\hat{\mathbf{E}}^{\text{inc}}, \hat{\mathbf{H}}^{\text{inc}}\}(x_1, x_3, j\omega; N) = \{\tilde{\mathbf{E}}_0^{\text{inc}}, \tilde{\mathbf{H}}_0^{\text{inc}}\}(x_1; N) \exp[-j(\beta x_3 - \omega t)]. \tag{5}$$

Here $N = \beta/k_0$ is the mode index or effective index, with β the (complex) propagation constant of the mode, and $k_0 = \omega/c$ the free-space wavenumber. In [3], a numerically stable method is described to obtain both the effective index and the field distribution in an active slab configuration, even when the background consists of layers with strong losses (i.e., $\text{Im}\{\epsilon\} < 0$).

From now on, the $j\omega$-dependence and the mode index N will be suppressed in our notation.

III. Domain Integral Equations

In this section, we derive domain integral equations which yield the field anywhere in the SLA. We distinguish between the actual configuration of Fig. 1 and the corresponding "background configuration." The latter consists of all layers but now *without* the finite gain domain $\mathcal{D}$, i.e., the layer $D^{(s)}$ with permittivity $\epsilon^{(s)}$ now extends all along x_3. The background, which is denoted by the superscript B, has scalar permittivity $\epsilon = \epsilon^B(x_1)$. In the configuration *with* the anisotropic domain $\mathcal{D}$, indicated with the superscript $\mathcal{D}$, we have $\epsilon = \epsilon_{ij}^{\mathcal{D}}(x_1, x_3)$.

We can write Maxwell's equations for the total field in the total configuration *with* the domain $\mathcal{D}$ by altering (2) and (3) into

$$-\nabla \times \hat{\mathbf{H}} + j\omega\epsilon^B \hat{\mathbf{E}} = -\hat{\mathbf{J}}^{\text{con}} \tag{6}$$

$$\nabla \times \hat{\mathbf{E}} + j\omega\mu_0 \hat{\mathbf{H}} = 0 \tag{7}$$

with

$$\hat{J}_m^{\text{con}}(x_1, x_3) \equiv j\omega[\epsilon_{mn}^{\mathcal{D}}(x_1, x_3) - \epsilon^B(x_1)\delta_{mn}] \times \hat{E}_n(x_1, x_3). \tag{8}$$

The "electric contrast source" $\hat{J}_m^{\text{con}}$ reflects the presence of the active volume $\mathcal{D}$ which has a different tensor permittivity $\epsilon_{mn}^{\mathcal{D}}$ within the embedding background. (The electric contrast current has the dimension of the time derivative of a polarization contrast. Therefore, it is sometimes called the "equivalent polarization current.") Everywhere outside D the contrast source vanishes. Notice that since we had assumed the magnetic permeability to be μ_0 everywhere, in this study we do not allow for contrast sources of the magnetic type.

Subtracting (2) and (3) for the incident field from (6) and (7) yields two expressions relating the scattered field and the total field

$$-\nabla \times \hat{\mathbf{H}}^{\text{sca}} + j\omega\epsilon^B \hat{\mathbf{E}}^{\text{sca}} = -\hat{\mathbf{J}}^{\text{con}} \tag{9}$$

$$\nabla \times \hat{\mathbf{E}}^{\text{sca}} + j\omega\mu_0 \hat{\mathbf{H}}^{\text{sca}} = 0. \tag{10}$$

The contrast source $\hat{J}_m^{\text{con}}$ can be written as a superposition of electric current line sources

$$\hat{J}_m^{\text{con}}(x_1, x_3) = \iint_{\mathcal{D}} \hat{J}_m^{\text{con}}(x_1', x_3')\delta(x_1 - x_1')\delta(x_3 - x_3')\, dx_1'\, dx_3'. \tag{11}$$

The scattered electric and magnetic fields that are generated by a single line source are the so-called Green states, symbolized by $\hat{\mathbf{E}}^G$ and $\hat{\mathbf{H}}^G$, respectively. From (9) and (10), it is clear that for a current line source at (x_1', x_3'), which is directed along a unit vector $\mathbf{a}$, the Green states satisfy

$$-\nabla \times \hat{\mathbf{H}}^G + j\omega\epsilon^B \hat{\mathbf{E}}^G = -\mathbf{a}\delta(x_1 - x_1')\delta(x_3 - x_3') \quad (12)$$

$$\nabla \times \hat{\mathbf{E}}^G + j\omega\mu_0 \hat{\mathbf{H}}^G = 0. \quad (13)$$

Obviously, both $\hat{\mathbf{E}}^G$ and $\hat{\mathbf{H}}^G$ are linearly related to $\mathbf{a}$. This relationship is expressed by the two Green tensors $\hat{G}^E$ and $\hat{G}^H$. That is, we define

$$\hat{E}_i^G = \hat{G}_{ij}^E\, a_j \quad (14)$$

$$\hat{H}_i^G = \hat{G}_{ij}^H\, a_j. \quad (15)$$

From the principle of superposition, it follows that the scattered electric field can be written as an integral

$$\hat{E}_m^{\text{sca}}(x_1, x_3) = \iint_{\mathcal{D}} \hat{G}_{mn}^E(x_1, x_3; x_1', x_3')\hat{J}_n^{\text{con}}(x_1', x_3')\, dx_1'\, dx_3'. \quad (16)$$

For the total electric field, we thus get [cf. (1)]

$$\hat{E}_m(x_1, x_3) = \hat{E}_m^{\text{inc}}(x_1, x_3) + j\omega \iint_{\mathcal{D}} \hat{G}_{mn}^E\, \Delta\epsilon_{np}(x_1', x_3') \times \hat{E}_p(x_1', x_3')\, dx_1'\, dx_3' \quad (17)$$

with

$$\Delta\epsilon_{np}(x_1, x_3) \equiv \epsilon_{np}^{\mathcal{D}}(x_1, x_3) - \epsilon^B(x_1)\delta_{np}. \quad (18)$$

In a completely similar manner, we find that

$$\hat{H}_m^{\text{sca}}(x_1, x_3) = \iint_{\mathcal{D}} \hat{G}_{mn}^H(x_1, x_3; x_1', x_3')\hat{J}_n^{\text{con}}(x_1', x_3')\, dx_1'\, dx_3'. \quad (19)$$

Hence, the total magnetic field is given by

$$\hat{H}_m(x_1, x_3) = \hat{H}_m^{\text{inc}}(x_1, x_3) + j\omega \iint_{\mathcal{D}} \hat{G}_{mn}^H\, \Delta\epsilon_{np}(x_1', x_3') \times \hat{E}_p(x_1', x_3')\, dx_1'\, dx_3'. \quad (20)$$

The integrals are over the domain $\mathcal{D}$ only. We now have two coupled domain integral equations for $\hat{E}_m$ and $\hat{H}_m$. Although the derived $\hat{\mathbf{E}}$ and $\hat{\mathbf{H}}$ fields in (17) and (20) are those of the total structure which contains the active region $\mathcal{D}$, it is of prime importance to note that the Green tensors $\hat{G}^E$ and $\hat{G}^H$ pertain to the relatively simple background configuration which does *not* contain $\mathcal{D}$. For $\mathbf{x} = (x_1, x_3) \in D$, (17) is a Fredholm equation of the second kind in $\hat{E}_m$. Once the Green tensor is known, the electric field can be solved numerically from (17). The solution can then be used in (20) to find the magnetic field.

Incidentally, one can also derive these domain integral equations from Lorentz's reciprocity theorem [11].

The derivation of the electric Green tensor $\hat{G}_{nm}^E$ is very involved and will be deferred to the Appendices. The magnetic Green tensor will not be derived since the magnetic field can be calculated by taking the curl of the electric field.

Equation (17) can be greatly simplified by using the Born approximation. The total field appearing in the integral is then replaced by the incident field, leading to

$$\hat{E}_m(x_1, x_3) \approx \hat{E}_m^{\text{inc}}(x_1, x_3) + j\omega \iint_{\mathcal{D}} \hat{G}_{mn}^E\, \Delta\epsilon_{np}(x_1', x_3') \times \hat{E}_p^{\text{inc}}(x_1', x_3')\, dx_1'\, dx_3'. \quad (21)$$

For points within the scattering domain, this means that the field is represented by the first term of the Born series. Rather than an integral equation, this is an integral that can be calculated numerically in a straightforward manner once the Green tensor is known. In Section V, we will compare the electric field in the Born approximation, (21), with the exact field given by (17).

IV. Discretization and Implementation

With the Green tensor known, and $\hat{\mathbf{E}}^{\text{inc}}$ given, we can now proceed to solve the integral (17). This will be done with the method of moments. Substituting the inverse Fourier transform of the Green's tensor into (17) gives

$$\hat{E}_m(x_1, x_3) = \hat{E}_m^{\text{inc}}(x_1, x_3) + \frac{j\omega}{2\pi} \iint_{\mathcal{D}} \times \left\{ \int_{-\infty}^{\infty} \tilde{G}_{mn} \exp[-jk_3(x_3 - x_3')]\, dk_3 \right\} \times \Delta\epsilon_{np}(x_1', x_3')\hat{E}_p(x_1', x_3')\, dx_1'\, dx_3'. \quad (22)$$

Next we write $\hat{E}_m$ as a sum of P expansion functions f_L

$$\hat{E}_m = \sum_{L=1}^{P} \alpha_{m;L}\, f_L(x_1, x_3) \quad (23)$$

with $\alpha_{m;L}$ expansion coefficients and $m = 1, 2, 3$. As weighting functions, we use the set $\{w_K(x_1, x_3)\}$ with $K = 1, \cdots, P$ which, just like f_L, have support $\mathcal{D}$. Expanding the field in (22), multiplying with w_K, and integrating over $\mathcal{D}$ yields

$$\sum_L (\alpha_{m;L}\, A_{KL} - \alpha_{p;L}\, C_{mp;KL}) = B_{m;K}, \quad (24)$$

where

$$A_{KL} = \iint_{\mathcal{D}} w_K(x_1, x_3) f_L(x_1, x_3)\, dx_1\, dx_3 \quad (25)$$

$$C_{mp;KL} = \frac{j\omega}{2\pi} \iint_{\mathcal{D}} w_K(x_1, x_3) \times \left[\iint_{\mathcal{D}} \left\{ \int_{-\infty}^{\infty} \tilde{G}_{mn} \exp[-jk_3(x_3 - x_3')]\, dk_3 \right\} \times \Delta\epsilon_{np}(x_1', x_3') f_L(x_1', x_3')\, dx_1'\, dx_3' \right] dx_1\, dx_3 \quad (26)$$

$$B_{m;K} = \iint_{\mathcal{D}} w_K(x_1, x_3) \hat{E}_m^{inc}(x_1, x_3)\, dx_1\, dx_3. \quad (27)$$

Next $\mathcal{D}$ is discretized into elements $\mathcal{D}_I$, with $I = 1, \cdots, P$. For the expansion functions f_I, we take hat functions with support $\mathcal{D}_I$, i.e.,

$$f_I(x_1, x_3) = \begin{cases} 1, & \text{if } (x_1, x_3) \in \mathcal{D}_I, \\ 0, & \text{otherwise} \end{cases} \quad (28)$$

and w_K is chosen to be the product of two delta functions

$$w_K = \delta(x_1 - x_{1K})\delta(x_3 - x_{3K}) \tag{29}$$

with (x_{1K}, x_{3K}) the baricenter of element $\mathcal{D}_K$. This choice of expansion functions and weighting functions is called the point-matching method, which leads to

$$A_{KL} = \delta_{KL} \tag{30}$$

$$C_{mp;KL} = \frac{j\omega}{2\pi} \iint_{\mathcal{D}_L} \left\{ \int_{-\infty}^{\infty} \tilde{G}_{mn}(x_{1K}, x_1'; k_3) \times \exp[-jk_3(x_{3K} - x_3')]\, dk_3 \right\} \times \Delta\epsilon_{np}(x_1', x_3')\, dx_1'\, dx_3' \tag{31}$$

$$B_{m;K} = \hat{E}_m^{inc}(x_{1K}, x_{3K}) \tag{32}$$

where δ_{KL} is the Kronecker symbol. Expression (31) for $C_{mp;KL}$ can be further simplified by assuming that $\Delta\epsilon_{np}$ is constant over $\mathcal{D}_L$. As is discussed at the end of Appendix B, the inner integral of (31) has no singularities. The outer integral has an integrable singularity. Therefore, according to Fubini's Theorem [15], we may interchange the order of integration which yields

$$C_{mp;KL} = \frac{j\omega}{2\pi} \Delta\epsilon_{np}(x_{1L}, x_{3L}) \int_{-\infty}^{\infty} T_{mn;KL}(k_3)\, dk_3 \tag{33}$$

with

$$T_{mn;KL}(k_3) = \frac{2}{k_3} \sin(k_3\Delta x_{3L}/2) \exp[-jk_3(x_{3K} - x_{3L})] \times \int_{\mathcal{D}_L} \tilde{G}_{mn}(x_{1K}, x_1'; k_3)\, dx_1' \tag{34}$$

where Δx_{3L} denotes the length along x_3 of the discretization element $\mathcal{D}_L$.

For all $(m, n; K, L)$, the tensor T can be determined analytically. From (85) for the Green's tensor, it is seen that for $n, m = 1, 2, 3$ there are only five out of nine combinations of n and m that yield nonzero elements of T.

From (24) it follows that the simultaneous linear equations for the expansion coefficients $\alpha_{m;L}$ of the total electric field can now be written in a matrix form as

$$(\mathcal{A} - \mathcal{C})\vec{\alpha} = \vec{\beta} \tag{35}$$

where

$$\vec{\alpha} = (\alpha_{1;1}, \cdots, \alpha_{1;P}, \alpha_{2;1}, \cdots, \alpha_{2;P}, \alpha_{3;1}, \cdots, \alpha_{3;P})^T \tag{36}$$

$$\vec{\beta} = (B_{1;1}, \cdots, B_{1;P}, B_{2;1}, \cdots, B_{2;P}, B_{3;1}, \cdots, B_{3;P})^T \tag{37}$$

$$\mathcal{A} = \begin{pmatrix} A_{11} & \cdots & A_{1P} & 0 & \cdots & 0 & 0 & \cdots & 0 \\ \vdots & & \vdots & \vdots & & \vdots & \vdots & & \vdots \\ A_{P1} & \cdots & A_{PP} & 0 & \cdots & 0 & 0 & \cdots & 0 \\ 0 & \cdots & 0 & A_{11} & \cdots & A_{1P} & 0 & \cdots & 0 \\ \vdots & & \vdots & \vdots & & \vdots & \vdots & & \vdots \\ 0 & \cdots & 0 & A_{P1} & \cdots & A_{PP} & 0 & \cdots & 0 \\ 0 & \cdots & 0 & 0 & \cdots & 0 & A_{11} & \cdots & A_{1P} \\ \vdots & & \vdots & \vdots & & \vdots & \vdots & & \vdots \\ \underbrace{0}_{P} & \cdots & \underbrace{0}_{P} & \underbrace{0}_{P} & \cdots & \underbrace{0}_{P} & \underbrace{A_{P1}}_{P} & \cdots & \underbrace{A_{PP}}_{P} \end{pmatrix} \tag{38}$$

and $\mathcal{C}$ is defined in (39), shown at the bottom of the page. From (30), it is seen that $\mathcal{A}$ is the $(3P \times 3P)$ identity matrix. The matrix $\mathcal{C}$, which contains the elements of the Green tensor, can be calculated from (33) and (83). The vector $\vec{\beta}$, which describes the distribution of the incident electric field, is supplied by a mode solver [3]. So, with all ingredients known, the simultaneous set of (35) for the field expansion coefficients $\vec{\alpha}$ can be solved.

The matrix elements in (39) are all combinations of the $9P^2$ tensor elements of $G_{mn;KL}$. However, because of the shift invariance of the background configuration along the propagation direction x_3, these tensor elements are not all independent. For instance, if P_1 denotes the discretization number of the domain $\mathcal{D}$ along the x_1 axis, then

$$G_{m,n;K,L} = G_{m,n;K+P_1,L+P_1}. \tag{40}$$

Exploiting this symmetry reduces the number of calculations needed to construct $\mathcal{C}$ from $\mathcal{O}(P^2)$ to $\mathcal{O}(P)$, where P denotes the total number of elements into which the domain $\mathcal{D}$ is divided.

$$\mathcal{C} = \begin{pmatrix} C_{11;11} & \cdots & C_{11;1P} & C_{12;11} & \cdots & C_{12;1P} & C_{13;11} & \cdots & C_{13;1P} \\ \vdots & & \vdots & \vdots & & \vdots & \vdots & & \vdots \\ C_{11;P1} & \cdots & C_{11;PP} & C_{12;P1} & \cdots & C_{12;PP} & C_{13;P1} & \cdots & C_{13;PP} \\ C_{21;11} & \cdots & C_{21;1P} & C_{22;11} & \cdots & C_{22;1P} & C_{23;11} & \cdots & C_{23;1P} \\ \vdots & & \vdots & \vdots & & \vdots & \vdots & & \vdots \\ C_{21;P1} & \cdots & C_{21;PP} & C_{22;P1} & \cdots & C_{22;PP} & C_{23;P1} & \cdots & C_{23;PP} \\ C_{31;11} & \cdots & C_{31;1P} & C_{32;11} & \cdots & C_{32;1P} & C_{33;11} & \cdots & C_{33;1P} \\ \vdots & & \vdots & \vdots & & \vdots & \vdots & & \vdots \\ \underbrace{C_{31;P1}}_{P} & \cdots & \underbrace{C_{31;PP}}_{P} & \underbrace{C_{32;P1}}_{P} & \cdots & \underbrace{C_{32;PP}}_{P} & \underbrace{C_{33;P1}}_{P} & \cdots & \underbrace{C_{33;PP}}_{P} \end{pmatrix} \tag{39}$$

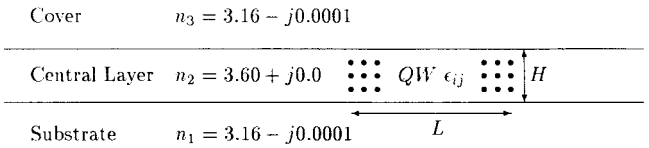

Fig. 2. A QW embedded in a lossy three-layer dielectric waveguide (side view). The wavelength in vacuum $\lambda_0 = 1.3\ \mu$m. The QW is situated in the central layer. It has a length L, height H, and permittivity ϵ_{ij}. The background configuration can only sustain one TE and one TM mode, which are both lossy.

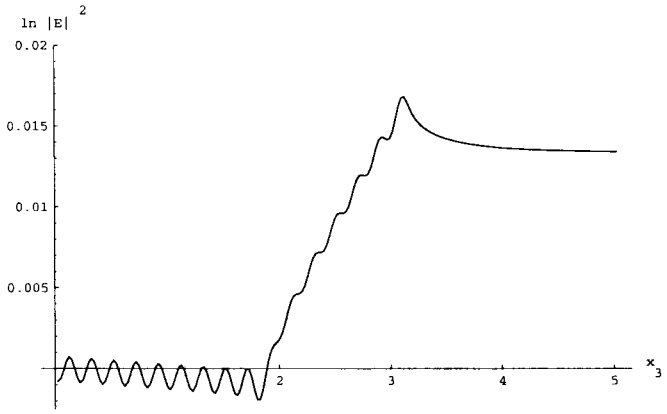

Fig. 3. Plot of $\ln |\mathbf{E}|^2$ around a QW that is embedded in the waveguiding structure of Fig. 2. The QW has a height of 150 nm and a length of $1.25\ \mu$m ($x_3 = 1.875\ \mu\text{m} < x_3 < 3.125\ \mu\text{m}$). The incident field travels in the positive x_3 direction and is TE polarized. In this example, $\lambda_0 = 1.3\ \mu$m, $\Delta\epsilon_{ij} = j0.03\,\delta_{ij}$.

V. Numerical Results

The numerical integration of (33) was carried out with routine D01AJF from the NAG library [16]. The simultaneous system of (35) was solved with routine F04ADF, also from the NAG library. The structure we examine, a QW embedded in a waveguide, is depicted in Fig. 2. Note that we use both refractive indices n and relative permittivities ϵ. The relation between the two is $\epsilon = n^2$.

An example of the intensity distribution in and around a QW embedded within this lossy layered background is shown in Fig. 3. In the region left of the QW ($x_3 < 1.875\ \mu$m), the incident TE field together with the reflected field give rise to a spatially oscillating intensity distribution with a decreasing maximum. Within the QW ($1.875\ \mu\text{m} < x_3 < 3.125\ \mu$m), the incident field gets amplified. Together with the counter propagating reflected field this gives a distribution which increases with x_3. In the region right of the QW ($x_3 > 3.125\ \mu$m), there is only a decreasing transmitted field. We note from (5) that, for a guided mode of the lossy background structure, $\ln |\mathbf{E}|^2$ is a decreasing linear function of the longitudinal coordinate x_3. It is seen from Fig. 3 that the transmitted field (i.e., the field to the right of the QW) gradually assumes this linear form. Note that this transition to a guided mode takes place over a length of approximately one effective wavelength. Using a less rigorous guided mode expansion, one does not obtain this structure of the near-field of the QW.

The field distribution around the QW is similar when the incident field is TM polarized; however, this field gets amplified less.

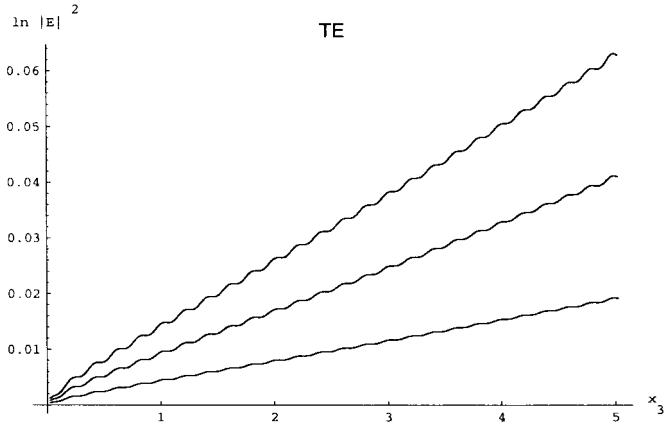

Fig. 4. Plot of $\ln |\mathbf{E}|^2$ as a function of position along the propagation direction x_3 (in micrometers) within a 5-μm-long QW. The QW is embedded in the waveguiding structure of Fig. 2. The incident field is TE polarized. The dielectric contrast tensor $\Delta\epsilon_{ij} = aj0.01\delta_{ij}$, with $a = 1$ (lower curve), $a = 2$ (middle curve), and $a = 3$ (upper curve). In this example, $H = 150$ nm, $L = 5\ \mu$m, and $\lambda_0 = 1.3\ \mu$m.

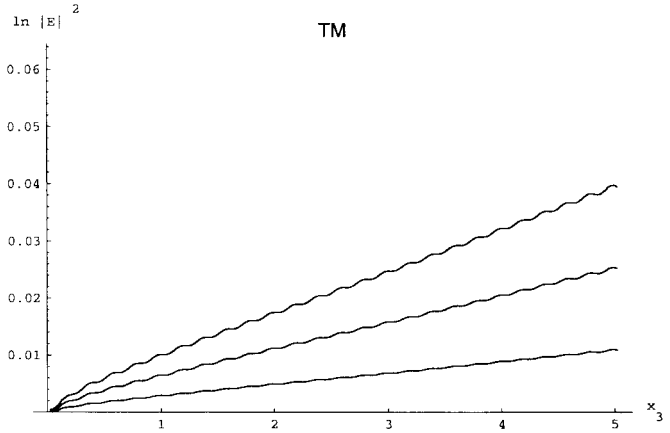

Fig. 5. Plot of $\ln |\mathbf{E}|^2$ as a function of position along the propagation direction x_3 (in micrometers) within a 5-μm-long QW. The QW is embedded in the waveguiding structure of Fig. 2. The incident field is TM polarized. The dielectric contrast tensor $\Delta\epsilon_{ij} = aj0.01\delta_{ij}$, with $a = 1$ (lower curve), $a = 2$ (middle curve), and $a = 3$ (upper curve). In this example, $H = 150$ nm, $L = 5\ \mu$m, $\lambda_0 = 1.3\ \mu$m.

The dependence of the amplification for incident TE waves on the dielectric contrast tensor is depicted in Fig. 4. Here $\Delta\epsilon_{ij} = aj0.01\delta_{ij}$, with $a = 1, 2, 3$. From the interference pattern one deduces that in the QW the effective wavelength $\lambda_{\text{eff}} = 0.4\ \mu$m. This agrees well with λ_{eff} of the incident field ($0.396\ \mu$m) which one expects to be hardly influenced by the relatively small dielectric contrast of the QW. We note that in all these cases the amplification is less than that of the corresponding active waveguide structure with an infinitely long QW.

The dependence of the amplification for incident TM waves on the dielectric contrast tensor is depicted in Fig. 5 for the same values. As expected (see Section I), the amplification is considerably less for this polarization state.

Thus far, we studied QW's with an isotropic contrast tensor, i.e., $\Delta\epsilon_{ij} = a\delta_{ij}$. Next we keep the off-diagonal tensor elements zero, but let the diagonal elements be different.

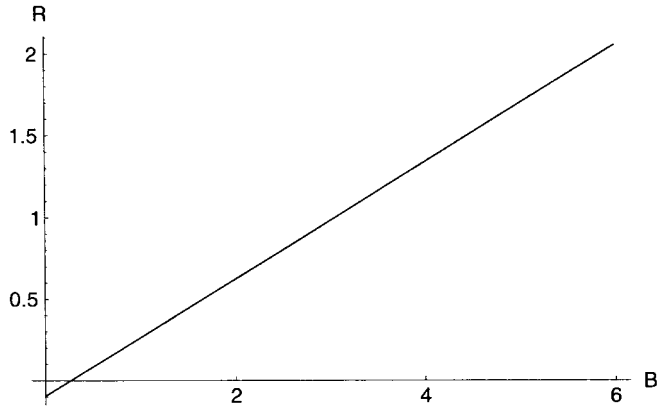

Fig. 6. Plot of $R = \ln |\mathbf{E}|^2_{\mathrm{TM}} / \ln |\mathbf{E}|^2_{\mathrm{TE}}$ at the end plane of the QW as a function of $\Delta\epsilon_{11}$. The 3-μm-long QW is embedded in the waveguiding structure of Fig. 2. The dielectric contrast tensor $\Delta\epsilon_{11} = Bj0.01$, with $0 < B < 6$. For $B \approx 3$, equal amplification for both polarization states is achieved. The other tensor elements were kept fixed at $\Delta\epsilon_{22} = \Delta\epsilon_{33} = j0.02$. In this example, $H = 150$ nm, $L = 3$ μm, and $\lambda_0 = 1.3$ μm.

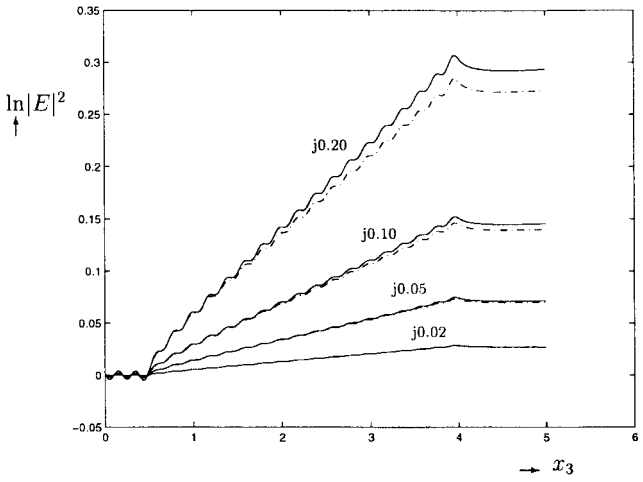

Fig. 7. Plot of $\ln |\mathbf{E}|^2$ as a function of position along the propagation direction x_3 (in micrometers) according to the exact integral equation (17) (solid line) and the Born approximation (21) (dashed line). The incident field is TE polarized. The dielectric contrast tensor is (from bottom upwards) $\Delta\epsilon_{ij} = j0.02\delta_{ij}$, $\Delta\epsilon_{ij} = j0.05\delta_{ij}$, $\Delta\epsilon_{ij} = j0.10\delta_{ij}$, and $\Delta\epsilon_{ij} = j0.20\delta_{ij}$. The 3.5-$\mu$m-long QW is embedded in the waveguiding structure of Fig. 2. In this example, $\lambda_0 = 1.3$ μm.

If we keep $\Delta\epsilon_{22}$ fixed, while varying $\Delta\epsilon_{11}$ and $\Delta\epsilon_{33}$, then the amplification of an incident TE wave remains unchanged. Likewise, for an incident TM wave, one can vary the value of $\Delta\epsilon_{22}$ without affecting its amplification. These results can be explained by considering the ith component of the first Maxwell equation for a source-free region:

$$-(\nabla \times \hat{H})_i + j\omega\epsilon_{ij}\hat{E}_j = 0. \tag{41}$$

For TE modes, only $\hat{E}_2$ is nonzero, whereas for TM modes both $\hat{E}_1$ and $\hat{E}_3$ are nonzero. So, from (41), it is seen that a change in ϵ_{11} or ϵ_{33} only affects the TM gain and leaves the TE gain unaltered. Since for TM modes $\hat{E}_1$ is the dominant electric field component, it is to be expected that a change in ϵ_{33} influences the TM gain to a lesser extent than a similar change in ϵ_{11}. Also, one expects that a change in ϵ_{22} only influences the TE gain. The above results agree with these deliberations.

Therefore, it appears that the TE gain and the TM gain can be influenced separately by influencing ϵ_{22} and ϵ_{11}, respectively. This gives us the opportunity to counteract the effect of waveguiding by introducing an anisotropy in the form of a uniaxial permittivity. That is, $\Delta\epsilon_{11} \neq \Delta\epsilon_{22} = \Delta\epsilon_{33}$. As before, the off-diagonal tensor elements are supposed to be zero. This is precisely the anisotropy that one would expect for a (001)-grown QW structure. To illustrate this, we took a 3-μm-long QW with $\Delta\epsilon_{22} = \Delta\epsilon_{33} = j0.02$ and varied $\Delta\epsilon_{11}$ (and therewith the TM gain, while keeping the TE gain constant). It was found that, for $\Delta\epsilon_{11} \approx j0.03$, equal amplification is obtained for both polarization states (see Fig. 6). So, for this particular configuration of QW and embedding, a polarization-independent operation of the amplifier can indeed be achieved. That this can also be realized under practical circumstances was demonstrated by Tiemeijer *et al.* [7]. The relationship between strain, optical transition matrix elements, and the dielectric tensor will be the subject of future studies.

The almost linear dependence of $\ln |\mathbf{E}|^2_{\mathrm{TM}}$ on $\Delta\epsilon_{11}$ indicates that in the weak contrast regime that we are considering the Born approximation is reasonably accurate. This can be seen from (21), according to which the scattered field (and hence, to a good approximation, $\ln |\mathbf{E}|^2$) varies linearly with $\Delta\epsilon$. The validity of the Born approximation is further investigated in Fig. 7 in which the field distribution around a QW is shown both according to the exact integral equation formalism (17) and the Born approximation (21). Two trends can be seen clearly: the Born approximation becomes less accurate for stronger scattering contrasts, and it becomes less accurate for points that lie further away from the front plane of the QW. Note that in all four cases the Born approximation underestimates the scattered field, as is to be expected for a gain medium. Also, in the Born approximation, we again see that the field behind the QW assumes the form of a guided mode of the background structure. That is, for $x_3 > 4$ μm, $\ln |\mathbf{E}|^2$ becomes a linear function of x_3. According to (5) this is typical for guided modes.

When off-axis elements in the permittivity contrast tensor are considered, one finds, as expected from (41), that TM/TE mixing takes place. That is, an incident TM field is not only reflected and amplified but now also gives rise to a reflected and a transmitted TE field, and vice versa. (Note that the dielectric tensor is always symmetric [17, Sec. 14.1].) As an example, we studied a purely imaginary contrast tensor with

$$\Delta\epsilon = \begin{pmatrix} j0.03 & j0.03 & 0 \\ j0.03 & j0.03 & 0 \\ 0 & 0 & j0.03 \end{pmatrix}. \tag{42}$$

In this case, about 6×10^{-6}% of the power of the incident TM mode was reflected as a TE signal. Of the transmitted (and amplified) signal, about 4×10^{-2}% was coupled to the TE mode.

VI. Conclusions

We have presented a model to analyze the propagation of polarized waves through a semiconductor laser amplifier

with an anisotropic QW. The model uses a rigorous scattering formalism for which the Green tensor for a layered structure with losses has been derived. It was found that the effects of waveguiding, which tend to favor the amplification of TE signals, can be compensated for by having an anisotropic uniaxial QW structure. The overall effect is then a polarization-insensitive amplification.

The use of an integral equation approach, although rigorous, means that the analysis is restricted to scatterers whose dimensions are less than about one hundred wavelengths. For larger sizes, the matrix equations become too large to handle. Nevertheless, we believe that the observed polarization sensitivity does not change when going to longer amplifier lengths (while staying in the linear regime).

With our model, one can study how the amplified field behind the QW gradually assumes the form of a guided mode of the embedding waveguide.

Also, the conversion of TE waves into TM waves due to off-diagonal elements of the permittivity tensor was analyzed.

A comparison between an exact expression for the scattered field and the Born approximation was made. It was found that, for the short ($\sim$5-μm) QW's in the weak contrast regime that we studied, the Born approximation is reasonably accurate. As expected, it systematically underestimates the field within the active region. Also, its accuracy decreases with higher contrast and greater length of the scattering structure.

Appendix A
The Electric Green Tensor for a Homogeneous Background

In this appendix, we first derive the electric Green tensor for a homogeneous background with permittivity ϵ. This permittivity is assumed to be a complex scalar. This corresponds with a background that is isotropic and lossy. The Green tensor can be found by determining the response of the background to a line source current, cf. (12) and (13). For $\mathbf{a} = x_p$, i.e., with the direction of the current line source along x_p ($p = 1, 2, 3$), the solution for the electric field is called as $\tilde{\mathbf{E}}^{G,p}$. It follows from (14) that it equals the pth column of the electric Green tensor. The background structure is invariant in the longitudinal or x_3 direction. We can take advantage of this by employing a Fourier transform

$$\tilde{G}(x_1; x_1', k_3) = \int_{-\infty}^{\infty} \hat{G}(x_1, x_3; x_1', x_3') \exp[jk_3(x_3 - x_3')]\, dx_3 \quad (43)$$

where we have dropped the superscript E. Both above and below the line source level $x_1 = x_1'$, the field quantities $\tilde{E}_2^{G,p}$, $\tilde{E}_3^{G,p}$, $\tilde{H}_2^{G,p}$, and $\tilde{H}_3^{G,p}$ can be expressed in terms of $\tilde{E}_1^{G,p}$ and $\tilde{H}_1^{G,p}$ by using the source-free Maxwell equations with $\partial_2 = 0$. It then follows that

$$(\partial_1^2 + {k_1}^2)\{\tilde{E}_1^{G,p}, \tilde{H}_1^{G,p}\} = 0, \qquad x_1 \neq x_1' \quad (44)$$

with $k_1 = [\omega^2\epsilon\mu_0 - {k_3}^2]^{1/2}$ and $\mathrm{Im}\{k_1\} \leq 0$. The solutions are exponential functions that must vanish for $|x_1| \to \infty$. The fields generated by the line source are now written as

$$\{\tilde{\mathbf{E}}^{G,p}, \tilde{\mathbf{H}}^{G,p}\} = \{\tilde{\mathcal{E}}, \tilde{\mathcal{H}}\}(-k_1, k_3) \cdot \mathbf{f}_p^+ \exp[-jk_1(x_1 - x_1')] \quad (45)$$

if $x_1 > x_1'$ and

$$\{\tilde{\mathbf{E}}^{G,p}, \tilde{\mathbf{H}}^{G,p}\} = \{\tilde{\mathcal{E}}, \tilde{\mathcal{H}}\}(+k_1, k_3) \cdot \mathbf{f}_p^- \exp[+jk_1(x_1 - x_1')] \quad (46)$$

if $x_1 < x_1'$. Here $\mathbf{f}_p^- = (f_{p,E}^-, f_{p,H}^-)^T$ and $\mathbf{f}_p^+ = (f_{p,E}^+, f_{p,H}^+)^T$ are the amplitudes of said exponentials that represent waves traveling in the negative and positive x_1 direction, respectively. The 3×2 coefficient matrices $\tilde{\mathcal{E}}$ and $\tilde{\mathcal{H}}$ that express all field components in terms of $\tilde{E}_1^{G,p}$ and $\tilde{H}_1^{G,p}$ are given by

$$\tilde{\mathcal{E}}(k_1, k_3) = \begin{pmatrix} 1 & 0 \\ 0 & -\omega\mu_0/k_3 \\ k_1/k_3 & 0 \end{pmatrix} \quad (47)$$

$$\tilde{\mathcal{H}}(k_1, k_3) = \begin{pmatrix} 0 & 1 \\ \omega\epsilon/k_3 & 0 \\ 0 & k_1/k_3 \end{pmatrix}. \quad (48)$$

The four components of $\mathbf{f}_p^-$ and $\mathbf{f}_p^+$ are determined by matching the fields at $x_1 = x_1'$. First, the components $\tilde{E}_1^{G,p}$ and $\tilde{H}_1^{G,p}$ are eliminated from Maxwell's equations with $J_i = \delta_{pi}\delta(x_1 - x_1')$, where δ_{pi} denotes the Kronecker symbol. (The reason being that these components are not differentiated with respect to x_1.) The resulting set of four first-order differential equations are integrated over an infinitesimally small interval that contains the source at x_1', which is directed along x_p. The result is

$$\begin{pmatrix} \tilde{E}_2^{G,p} \\ \tilde{E}_3^{G,p} \\ \tilde{H}_2^{G,p} \\ \tilde{H}_3^{G,p} \end{pmatrix}(x_1 \downarrow x_1') - \begin{pmatrix} \tilde{E}_2^{G,p} \\ \tilde{E}_3^{G,p} \\ \tilde{H}_2^{G,p} \\ \tilde{H}_3^{G,p} \end{pmatrix}(x_1 \uparrow x_1') = \begin{pmatrix} 0 \\ (k_3/\omega\epsilon)\delta_{p1} \\ \delta_{p3} \\ -\delta_{p2} \end{pmatrix}. \quad (49)$$

Combining (45) and (46) while using (49) yields the solution for $\mathbf{f}_p^{\pm}$ with $p = 1, 2, 3$

$$\mathbf{f}_1^+ = \mathbf{f}_1^- = \begin{pmatrix} -{k_3}^2/2\omega\epsilon k_1 \\ 0 \end{pmatrix} \quad (50)$$

$$\mathbf{f}_2^+ = \mathbf{f}_2^- = \begin{pmatrix} 0 \\ k_3/2k_1 \end{pmatrix} \quad (51)$$

$$\mathbf{f}_3^+ = -\mathbf{f}_3^- = \begin{pmatrix} k_3/2\omega\epsilon \\ 0 \end{pmatrix}. \quad (52)$$

With the $\mathbf{f}$ vectors known, we can solve Maxwell's equations with a current line source using (45) and (46). As argued above, for each choice (x_1, x_2, x_3) for the current direction p, the resulting electric field $\tilde{\mathbf{E}}^{G,p}$ is identical with the pth

column of the electric Green tensor. The tensor can be written as the sum of a singular part and a regular part. This gives

$$\tilde{\mathbf{G}}(x_1, x_1'; k_3) = \tilde{\mathbf{G}}^s \delta(x_1 - x_1') + \tilde{\mathbf{G}}^r(k_1, k_3) \exp(-jk_1|x_1 - x_1'|) \quad (53)$$

with

$$\tilde{\mathbf{G}}^s = \frac{-1}{j\omega\epsilon} \begin{pmatrix} 1 & 0 & 0 \\ 0 & 0 & 0 \\ 0 & 0 & 0 \end{pmatrix} \quad (54)$$

and

$$\tilde{\mathbf{G}}^r = \frac{1}{2\omega\epsilon} \begin{pmatrix} -k_3^2/k_1 & 0 & Sk_3 \\ 0 & -(k_1{}^2 + k_3{}^2)/k_1 & 0 \\ Sk_3 & 0 & -k_1 \end{pmatrix}. \quad (55)$$

Here $S = \text{sign}(x_1 - x_1')$. Notice that the above derivation is also valid if the homogeneous background is lossy, i.e., it has a complex index of refraction.

Appendix B
The Electric Green Tensor for a Multilayered Background

Consider the layered background configuration corresponding to the structure of Fig. 1. The line source current is supposed to be located within layer $D^{(s)}$. Within each source-free layer $D^{(n)}$, we can again express all field quantities in terms of $\tilde{E}_1^{G,p}$ and $\tilde{H}_1^{G,p}$, cf. (45) and (46)

$$\{\tilde{\mathbf{E}}^{G,p}, \tilde{\mathbf{H}}^{G,p}\} = \{\tilde{\mathcal{E}}, \tilde{\mathcal{H}}\}(-k_1^n, k_3) \cdot \mathbf{f}_p^{n,+} \exp[-jk_1^n(x_1 - x_1^{n,\text{ref}})] + \{\tilde{\mathcal{E}}, \tilde{\mathcal{H}}\}(+k_1^n, k_3) \cdot \mathbf{f}_p^{n,-} \exp[+jk_1^n(x_1 - x_1^{n,\text{ref}})] \quad (56)$$

with $k_1^n = [\omega^2\epsilon^n\mu_0 - k_3{}^2]^{1/2}$ and $\text{Im}\{k_1^n\} \leq 0$. The amplitude vectors $\mathbf{f}_p^{n,-} = (f_{p,E}^{n,-}, f_{p,H}^{n,-})^T$ and $\mathbf{f}_p^{n,+} = (f_{p,E}^{n,+}, f_{p,H}^{n,+})^T$ are now layer-dependent. The matrices $\tilde{\mathcal{E}}$ and $\tilde{\mathcal{H}}$ are still given by (47) and (48). For a layer $D^{(n)}$ above the source level $x_1 = x_1'$, the reference level $x_1^{n,\text{ref}}$ is taken at the lower interface of the layer, i.e., $x_1^{n,\text{ref}} = x^{n-1}$. For layers below the source level, we put $x_1^{n,\text{ref}} = x^n$. The line source problem is solved once we have determined the $\mathbf{f}$ vectors in all layers, as we shall now do.

In the superstrate and substrate, the fields must decay exponentially. This gives the boundary conditions

$$\mathbf{f}_p^{N+1,-} = \mathbf{f}_p^{1,+} = \begin{pmatrix} 0 \\ 0 \end{pmatrix}. \quad (57)$$

The tangential field components are continuous across the interfaces of the background configuration. This leads to a condition for $\tilde{\mathcal{E}}_T$ and $\tilde{\mathcal{H}}_T$ which are defined as the lower 2×2 submatrices of $\tilde{\mathcal{E}}$ and $\tilde{\mathcal{H}}$, respectively. For example, for the interface between the layers $D^{(n)}$ and $D^{(n+1)}$, the continuity condition reads

$$\mathbf{Q}^{(n+1)}(x_1^n) \begin{pmatrix} \mathbf{f}_p^{n+1,+} \\ \mathbf{f}_p^{n+1,-} \end{pmatrix} = \mathbf{Q}^{(n)}(x_1^n) \begin{pmatrix} \mathbf{f}_p^{n,+} \\ \mathbf{f}_p^{n,-} \end{pmatrix}. \quad (58)$$

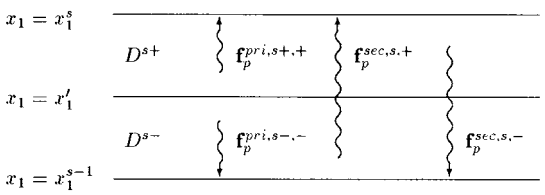

Fig. 8. The primary and secondary amplitude vectors.

Here the 4×4 matrix $\mathbf{Q}^{(n)}$ is given by

$$\mathbf{Q}^{(n)}(x_1) \equiv \begin{pmatrix} \tilde{\mathcal{E}}_T(-k_1^n, k_3)/\text{EXP} & \tilde{\mathcal{E}}_T(+k_1^n, k_3)\,\text{EXP} \\ \tilde{\mathcal{H}}_T(-k_1^n, k_3)/\text{EXP} & \tilde{\mathcal{H}}_T(+k_1^n, k_3)\,\text{EXP} \end{pmatrix} \quad (59)$$

where $\text{EXP} \equiv \exp[jk_1^n(x_1 - x_1^{n,\text{ref}})]$.

We can consider the layer $D^{(s)}$, which contains the line source, to be made up of two source-free layers called D^{s+} and D^{s-}, that are situated above and below the line source at $x_1 = x_1'$, respectively. The field can now be written as a sum of a known primary field (which takes the line source into account) and a secondary field which represents the multiple reflections at the various interfaces (see Fig. 8). With the notation of (56), the primary amplitude vectors $\mathbf{f}_p^{\text{pri},\,s\pm,\pm}$ in D^{s+} and D^{s-} are given by (50)–(52). The primary, secondary, and total amplitude vectors are interrelated through

$$\mathbf{f}_p^{s+,+} = \mathbf{f}_p^{\text{pri},\,s+,+} + \mathbf{f}_p^{\text{sec},\,s,+} \quad (60)$$

$$\mathbf{f}_p^{s+,-} = \quad + \mathbf{f}_p^{\text{sec},\,s,-} \quad (61)$$

$$\mathbf{f}_p^{s-,+} = \quad + \mathbf{f}_p^{\text{sec},\,s,+} \quad (62)$$

$$\mathbf{f}_p^{s-,-} = \mathbf{f}_p^{\text{pri},\,s-,-} + \mathbf{f}_p^{\text{sec},\,s,-}. \quad (63)$$

Notice that the primary fields always travel away from the line source. Elimination of the secondary amplitude vectors yields the excitation conditions

$$\mathbf{f}_p^{s+,+} = \mathbf{f}_p^{\text{pri},\,s+,+} + \mathbf{f}_p^{s-,+}$$
$$\mathbf{f}_p^{s-,-} = \mathbf{f}_p^{\text{pri},\,s-,-} + \mathbf{f}_p^{s+,-}. \quad (64)$$

The solution of the line source problem is uniquely determined by the boundary, continuity, and excitation conditions, as we will now show.

In our formalism, the reference vectors in subsequent layers are related by the continuity condition across the interface. For layers above the line source, a downward recursion scheme is applied, whereas an upward recursion scheme is used for layers below the line source. Both schemes are then matched at the source level using the excitation conditions.

The transmission coefficient $t_i^{d,n}$ and the reflection coefficient $r_i^{d,n}$ for a layer $D^{(n)}$ above the source level are defined as

$$f_{p,i}^{N+1,+} = t_i^{d,n} f_{p,i}^{n,+}, \qquad f_{p,i}^{n,-} = r_i^{d,n} f_{p,i}^{n,+}. \quad (65)$$

The superscript d denotes downward recursion, and the subscript $i = E, H$ indicates which component of $\mathbf{f}$ we are dealing with [see (56)]. The reflection and transmission coefficients of layer $D^{(n)}$ are expressed recursively in those of

layer $D^{(n+1)}$. This is done by using the continuity condition (58) at the interface $x_1 = x_1^{(n)}$. This gives

$$t_H^{d,n} = \frac{2\,t_H^{d,n+1}\,\gamma k_1^n}{k_1^{n+1}(1-r_H^{d,n+1}) + k_1^n(1+r_H^{d,n+1})} \tag{66}$$

$$r_H^{d,n} = -\gamma^2 \frac{k_1^{n+1}(-1+r_H^{d,n+1}) + k_1^n(1+r_H^{d,n+1})}{k_1^{n+1}(-1+r_H^{d,n+1}) - k_1^n(1+r_H^{d,n+1})} \tag{67}$$

$$r_E^{d,n} = -\gamma^2 \frac{\epsilon^n\,k_1^{n+1}(-1+r_E^{d,n+1}) + \epsilon^{n+1}\,k_1^n(1+r_E^{d,n+1})}{\epsilon^n\,k_1^{n+1}(-1+r_E^{d,n+1}) - \epsilon^{n+1}\,k_1^n(1+r_E^{d,n+1})} \tag{68}$$

$$t_E^{d,n} = \frac{2\,t_E^{d,n+1}\,\gamma\,k_1^n\,\epsilon^n}{\epsilon^n\,k_1^{n+1}\,(1-r_E^{d,n+1}) + \epsilon^{n+1}\,k_1^n(1+r_E^{d,n+1})} \tag{69}$$

where $\gamma \equiv \exp[-jk_1^n(x_1^n - x_1^{n-1})]$. The scheme for determining the reflection and transmission coefficients is initialized by taking as their values in the cover

$$t_i^{d,N+1} = 1, \qquad r_i^{d,N+1} = 0. \tag{70}$$

These two conditions express the transparency of the superstrate for the wave constituents.

Similarly, for a layer $D^{(n)}$ below the line source level, we define

$$f_{p,i}^{1,-} = t_i^{u,n}\,f_{p,i}^{n,-}, \qquad f_{p,i}^{n,+} = r_i^{u,n}\,f_{p,i}^{n,-} \tag{71}$$

where the superscript u denotes upward recursion. The reflection and transmission coefficients of layer $D^{(n+1)}$ are expressed recursively in those of layer $D^{(n)}$. Using the continuity condition at the interface $x_1 = x_1^{(n-1)}$ yields

$$r_H^{u,n+1} = -\delta^2\,\frac{k_1^n(1-r_H^{u,n}) - k_1^{n+1}(1+r_H^{u,n})}{k_1^n(1-r_H^{u,n}) + k_1^{n+1}(1+r_H^{u,n})} \tag{72}$$

$$t_H^{u,n+1} = \frac{2\,t_H^{u,n}\,\delta k_1^{n+1}}{k_1^n(1-r_H^{u,n}) + k_1^{n+1}(1+r_H^{u,n})} \tag{73}$$

$$r_E^{u,n+1} = -\delta^2\,\frac{\epsilon^{n+1}\,k_1^n(-1+r_E^{u,n}) + \epsilon^n\,k_1^{n+1}(1+r_E^{u,n})}{\epsilon^{n+1}\,k_1^n(-1+r_E^{u,n}) - \epsilon^n\,k_1^{n+1}(1+r_E^{u,n})} \tag{74}$$

$$t_E^{u,n+1} = \frac{2\,t_E^{u,n}\delta\epsilon^{n+1}\,k_1^{n+1}}{\epsilon^{n+1}\,k_1^n(1-r_E^{u,n}) + \epsilon^n\,k_1^{n+1}(1+r_E^{u,n})} \tag{75}$$

where $\delta \equiv \exp[-jk_1^{n+1}(x_1^{n+1} - x_1^n)]$. The upward recursion scheme is initialized by taking for the reflection and transmission coefficients in the substrate

$$t_i^{u,1} = 1, \qquad r_i^{u,1} = 0. \tag{76}$$

These two conditions express the transparency of the substrate for the wave constituents. Notice that both recursion schemes are independent of the direction p of the current line source. The two schemes combined give us the reflection coefficients for the layers D^{s+} and D^{s-}

$$f_{p,i}^{s+,-} = r_i^{d,s+}\,f_{p,i}^{s+,+}, \qquad f_{p,i}^{s-,+} = r_i^{u,s-}\,f_{p,i}^{s-,-}. \tag{77}$$

Using (77) in the two excitation conditions (64) allows us to solve for $f_{p,i}^{s+,+}$ and $f_{p,i}^{s-,-}$. The result is

$$f_{p,i}^{s+,+} = (f_{p,i}^{\mathrm{pri},\,s+,+} + r_i^{u,\,s-}\,f_{p,i}^{\mathrm{pri},\,s-,-})/(1 - r_i^{u,\,s-}r_i^{d,\,s+}) \tag{78}$$

$$f_{p,i}^{s-,-} = (f_{p,i}^{\mathrm{pri},\,s-,-} + r_i^{d,\,s+}\,f_{p,i}^{\mathrm{pri},\,s+,+})/(1 - r_i^{u,\,s-}\,r_i^{d,\,s+}). \tag{79}$$

With (77)–(79), the $\mathbf{f}$ vectors for layer $D^{(s)}$ are expressed in the known primary fields f^{pri}. By (65) and (71), the $\mathbf{f}$ vectors in any other layer (and hence the total field) are determined while explicitly satisfying the boundary conditions (57), the continuity conditions (58), and the excitation conditions (64).

Let r_i^{d*} be the reflection coefficient of layer D^{s+} in the downward recursive scheme for a line source current situated at $x_1' = 0 = (x_1^s + x_1^{s-1})/2$. Also, let r_i^{u*} be the reflection coefficient of layer D^{s-} in the upward recursive scheme for a line source current situated at $x_1' = 0$

$$r_i^{d*} = r_i^{d,\,s+}(x_1' = 0), \qquad r_i^{u*} = r_i^{u,\,s-}(x_1' = 0). \tag{80}$$

From (67), (68), (72), and (74), it then follows that if the line source is located elsewhere in layer $D^{(s)}$ the thickness of D^{s+} and D^{s-} changes and hence

$$r_i^{d,\,s+}(x_1') = r_i^{d*}\,\exp[2jk_1^s\,x_1'], \tag{81}$$

$$r_i^{u,\,s-}(x_1') = r_i^{u*}\,\exp[-2jk_1^s\,x_1']. \tag{82}$$

For $p = (x_1, x_2, x_3)$, the solution for the amplitude vectors of (77)–(79) together with the general solution of the electric field (56) are substituted in Maxwell's equations (with line source along x_p). These are then solved for the electric field. This field corresponds with column number $(1, 2, 3)$ of the electric Green tensor, respectively. The result is again the sum of a singular and a regular part

$$\tilde{\mathbf{G}}(x_1, x_1'; k_3) = \tilde{\mathbf{G}}^s\,\delta(x_1 - x_1') + \tilde{\mathbf{G}}^r \tag{83}$$

with

$$\tilde{\mathbf{G}}^s = \frac{-1}{j\omega\epsilon^s}\begin{pmatrix} 1 & 0 & 0 \\ 0 & 0 & 0 \\ 0 & 0 & 0 \end{pmatrix} \tag{84}$$

and

$$\tilde{\mathbf{G}}^r = \frac{1}{2\omega\epsilon^s}\begin{pmatrix} -k_3^2\,a/k_1^s & 0 & k_3\,b \\ 0 & -k^{s^2}\,c/k_1^s & 0 \\ k_3\,d & 0 & -k_1^s\,e \end{pmatrix} \tag{85}$$

where

$$a = \exp[jk_1^s(x_1 - x_1')]\,(\exp(2jk_1^s\,x_1') + r_E^{u*}) \times (\exp(-2jk_1^s\,x_1) + r_E^{d*})/D_E \tag{86}$$

$$b = \exp[jk_1^s(x_1 - x_1')]\,(\exp(2jk_1^s\,x_1') - r_E^{u*}) \times (\exp(-2jk_1^s\,x_1) + r_E^{d*})/D_E \tag{87}$$

$$c = \exp[jk_1^s(x_1 - x_1')]\,(\exp(2jk_1^s\,x_1') + r_H^{u*}) \times (\exp(-2jk_1^s\,x_1) + r_H^{d*})/D_H \tag{88}$$

$$d = \exp[jk_1^s(x_1 - x_1')]\,(\exp(2jk_1^s\,x_1') + r_E^{u*}) \times (\exp(-2jk_1^s\,x_1) - r_E^{d*})/D_E \tag{89}$$

$$e = \exp[jk_1^s(x_1 - x_1')]\,(\exp(2jk_1^s\,x_1') - r_E^{u*}) \times (\exp(-2jk_1^s\,x_1) - r_E^{d*})/D_E \tag{90}$$

if $x_1 > x_1'$. Here $D_i = 1 - r_i^{u*} r_i^{d*}$ with $i = E, H$, and

$$a = \exp[jk_1^s(x_1' - x_1)]\,(+\exp(2jk_1^s x_1) + r_E^{u*}) \times (+\exp(-2jk_1^s x_1') + r_E^{d*})/D_E \quad (91)$$

$$b = \exp[jk_1^s(x_1' - x_1)]\,(+\exp(2jk_1^s x_1) + r_E^{u*}) \times (-\exp(-2jk_1^s x_1') + r_E^{d*})/D_E \quad (92)$$

$$c = \exp[jk_1^s(x_1' - x_1)]\,(+\exp(2jk_1^s x_1) + r_H^{u*}) \times (+\exp(-2jk_1^s x_1') + r_H^{d*})/D_H \quad (93)$$

$$d = \exp[jk_1^s(x_1' - x_1)]\,(-\exp(2jk_1^s x_1) + r_E^{u*}) \times (+\exp(-2jk_1^s x_1') + r_E^{d*})/D_E \quad (94)$$

$$e = \exp[jk_1^s(x_1' - x_1)]\,(-\exp(2jk_1^s x_1) + r_E^{u*}) \times (-\exp(-2jk_1^s x_1') + r_E^{d*})/D_E \quad (95)$$

if $x_1 < x_1'$. The functions a through e all have as arguments (x_1, x_1', k_3). Notice that the above derivation is also valid when the background layers have a complex index of refraction.

The Green tensor has two types of singularities in the complex k_3-plane. The factor $D_i(k_3)$ vanishes if k_3 equals a (complex) propagation constant of the background configuration. Also, the tensor has branch points $k_3 = \pm k^s$ because k_1^s is defined as a complex root [see (44)]. If the background is lossy, these singularities will not lie on the real k_3 axis. There are *no* singularities in $k_1^s(k_3)$. It can be shown that $k_1^s(k_3)$, just like $k_1(k_3)$ of all intermediate layers, has no branch points in the complex k_3 plane [18].

ACKNOWLEDGMENT

The authors wish to thank A. Leefers for implementing the Born approximation.

REFERENCES

[1] P. Wysocki and V. Mazurczyk, "Polarization-dependent gain in Erbium-doped fiber amplifiers: Computer model and approximate formulas," *J. Lightwave Technol.*, vol. 14, pp. 572–584, 1996.

[2] J. L. Wagener, D. G. Falquier, M. J. F. Digonnet, and H. J. Shaw, "A Mueller matrix formalism for modeling polarization effects in Erbium-doped fiber," *J. Lightwave Technol.*, vol. 16, pp. 200–206, 1998.

[3] T. D. Visser, H. Blok, and D. Lenstra, "Modal analysis of a planar waveguide with gain and losses," *IEEE J. Quantum Electron.*, vol. 31, pp. 1803–1810, 1995.

[4] T. D. Visser, B. Demeulenaere, J. Haes, D. Lenstra, R. Baets, and H. Blok, "Confinement and modal gain in dielectric waveguides," *J. Lightwave Technol.*, vol. 14, pp. 885–887, 1996.

[5] T. D. Visser, H. Blok, B. Demeulenare, and D. Lenstra, "Confinement factors and gain in optical amplifiers," *IEEE J. Quantum Electron.*, vol. 33, pp. 1763–1766, 1997.

[6] B. Mersali, L. F. Tiemijer, P. F. A. Thijs, T. van Dongen, R. W. M. Slootweg, and F. F. M. van der Heijden, "1.55 high gain polarization insensitive semiconductor traveling wave amplifier with low driving current," *Electron. Lett.*, vol. 26, pp. 124–125, 1990.

[7] L. F. Tiemeijer, P. F. A. Thijs, T. van Dongen, R. W. M. Slootweg, and F. F. M. van der Heijden, "Polarization insensitive multiple quantum well laser amplifiers for the 1300 nm window," *Appl. Phys. Lett.*, vol. 62, pp. 826–828, 1993.

[8] ——, "Polarization resolved, complete characterization of 1310 nm fiber pigtailed multiple-quantum-well optical amplifiers," *J. Lightwave Technol.*, vol. 14, pp. 1524–1533, 1996.

[9] E. W. Kolk, N. H. G. Baken, and H. Blok, "Domain integral equation analysis of integrated optical channel and ridge waveguides in stratified media," *IEEE Trans. Microwave Theory Tech.*, vol. 38, pp. 78–85, 1990.

[10] N. H. G. Baken, M. B. J. Diemeer, J. M. van Splunter, and H. Blok, "Computational modeling of diffused channel waveguides using a domain integral equation," *J. Lightwave Technol.*, vol. 8, pp. 576–586, 1990.

[11] N. H. G. Baken, "Computational modelling of integrated-optical waveguides," Ph.D. dissertation, Technical University Delft, Delft, The Netherlands, 1990.

[12] H. J. M. Bastiaansen, "Modal analysis of straight and curved integrated optical waveguides," Ph.D. dissertation, Technical University Delft, Delft, The Netherlands, 1994.

[13] K. S. Chiang, "Review of numerical and approximate methods for the modal analysis of general optical dielectric waveguides," *Opt. Quantum Electron.*, vol. 26, pp. S113–S134, 1994.

[14] R. J. Hawkins and J. S. Kalman, "Lasing in tilted-waveguide semiconductor laser amplifiers," *Opt. Quantum Electron.*, vol. 26, pp. S207–S219, 1994.

[15] A. N. Kolomogorov and S. V. Fomin, *Introductory Real Analysis.* New York: Dover, 1975.

[16] Numerical Algorithm Group Ltd., Oxford, UK.

[17] M. Born and E. Wolf, *Principles of Optics*, 6th ed. Oxford, U.K.: Pergamon Press, 1980.

[18] W. C. Chew, *Waves and Fields in Inhomogeneous Media.* New York: IEEE Press, 1995, p. 112.

T. D. Visser received the Ph.D. degree from the University of Amsterdam, Amsterdam, The Netherlands, in 1992.

He is now an Assistant Professor of Theoretical Physics at the Free University in Amsterdam, Amsterdam. His research interests are semiconductor lasers and amplifiers and the theory of diffraction and scattering.

H. Blok is a Professor of Electromagnetics at Delft University of Technology, Delft, The Netherlands. His research focuses on beam propagation methods, integrated optics, and inverse scattering theory.

D. Lenstra is a Professor of Theoretical Physics and Dean of the Department of Physics and Astronomy at the Free University in Amsterdam, Amsterdam, The Netherlands. He conducts research on various aspects of semiconductor lasers such as nonlinear dynamics, wave propagation, and quantum electrodynamics.